Preoperative Assessment of Intracranial Tumors with Perfusion MR and a Volumetric Interpolated Examination: A Comparative Study with DSA

Stephan G. Wetzel, Soonmee Cha, Meng Law, Glyn Johnson, John Golfinos, Peter Lee, and Peter Kim Nelson

BACKGROUND AND PURPOSE: In evaluating intracranial tumors, a safe low-cost alternative that provides information similar to that of digital subtraction angiography (DSA) may be of interest. Our purpose was to determine the utility and limitations of a combined MR protocol in assessing (neo-) vascularity in intracranial tumors and their relation to adjacent vessels and to compare the results with those of DSA.

METHODS: Twenty-two consecutive patients with an intracranial tumor who underwent preoperative stereoscopic DSA were examined with contrast-enhanced dynamic T2*-weighted perfusion MR imaging followed by a T1-weighted three-dimensional (3D) MR study (volumetric interpolated brain examination [VIBE]). The maximum relative cerebral blood volume (rCBV) of the tumor was compared with tumor vascularity at DSA. Critical vessel structures were defined in each patient, and VIBE images of these structures were compared with DSA findings. For full exploitation of the 3D data sets, maximum-intensity projection algorithms reconstructed in real time with any desired volume and orientation were used.

RESULTS: Tumor blush scores at DSA were significantly correlated with the rCBV measurements ($r = 0.75$; $P < .01$, Spearman rank correlation coefficient). In 17 (77%) patients, VIBE provided all relevant information about the venous system, whereas information about critical arteries were partial in 50% of the cases and not relevant in the other 50%.

CONCLUSION: A fast imaging protocol consisting of perfusion MR imaging and a volumetric MR acquisition provides some of the information about tumor (neo-) vascularity and adjacent vascular anatomy that can be obtained with conventional angiography. However, the MR protocol provides insufficient visualization of distal cerebral arteries.

CT and, more recently, MR imaging, have supplanted conventional angiography as the primary imaging tools for the diagnosis and localization of intracranial tumors. However, digital subtraction angiography (DSA) may still be valuable for the preoperative workup of patients with intracranial tumors, because it can provide information not readily available with conventional MR imaging. First, tumor (neo-) vascularity, which can be important for tumor grading, is demonstrated by DSA. Second, DSA is still the standard of reference for defining the normal vascular anatomy in relation to the tumor. Knowledge of the venous anatomy is particularly important for minimizing the risk of vascular injury in planning biopsy or resection of the tumor (1). However, DSA is time consuming, expensive, and invasive (2), and it is probably not part of the routine evaluation of patients with intracranial neoplasms in most radiologic centers worldwide. Although we are not aware of any cost-benefit analyses of presurgical DSA as an adjunct to MR imaging, we suspect that many centers do not use DSA, because they believe that the disadvantages outweigh the advantages. A safe, low-cost alternative that provides information similar to that of DSA may therefore be of interest.

Recent MR developments provide the means to assess both tumoral (neo-) vascularity and the normal cerebral vessels without the inherent drawbacks of

DSA. First, dynamic contrast-enhanced perfusion MR imaging (pMRI) is increasingly used to assess vascularity in brain tumors, and it has been used to determine the grade and malignancy of the tumor (3–8). Second, improvements in T1-weighted three-dimensional (3D) gradient-echo (GRE) MR imaging allow the rapid acquisition of high-spatial-resolution data sets of the whole brain. Used in combination with contrast agents, these sequences enable evaluations of both the cerebral vasculature and the brain parenchyma.

At our institution, presurgical conventional stereoscopic angiography is still performed as a routine examination in patients undergoing tumor resection or stereotactic biopsy. We compared the presurgical angiographic findings from 22 patients with findings from a combined MR control protocol consisting of a T2*-weighted pMRI examination immediately followed by a 3D T1-weighted contrast-enhanced MR imaging study. The 3D sequence used was optimized for short acquisition times and resolution improvements through the use of asymmetric k-space sampling and interpolation (9). Interactive, real-time maximum-intensity projection (MIP) algorithms used in conjunction with source images were used to fully exploit the 3D data sets.

We hypothesized that a combination of these MR techniques has the potential to provide information about 1) tumor (neo-) vascularity and 2) the vascular anatomy of importance to a neurosurgeon and that would normally be obtained from the conventional angiographic study.

Methods

Patients and Protocol

Twenty-two patients with brain tumors were examined during a 3-month period. Stereoscopic DSA and conventional MR imaging with pMRI were performed in these patients as part of the standard evaluation at our institution. In addition, contrast-enhanced T1-weighted 3D imaging was performed. Patients who were unable to undergo extended imaging because of severe claustrophobia or discomfort and patients undergoing MR spectroscopy (which would have prolonged the examination time) were excluded from the study. Otherwise, the patients were consecutive. All patients underwent MR examination and DSA examination on the same day, and neurosurgery was performed within 3 days of the radiologic examination (in 19 patients, within 1 day). Informed consent was obtained from all patients before participating in the study.

MR Equipment, Sequences, and Parameters

All examinations were performed with a 1.5-T clinical imaging system (Magnetom Vision; Siemens Medical Systems, Iselin, NJ) equipped with high-performance gradients.

Perfusion MR Imaging.—Perfusion data were acquired with a lipid-suppressed T2*-weighted echo-planar imaging sequence with the following parameters: TR/TE, 1000/54; FOV, 230 × 230 mm; section thickness, 5 or 7 mm; data matrix, 128 × 128; and in-plane voxel size, 1.8 × 1.8 mm. Five to seven sections were obtained with a gap of 0–30% of the section thickness to cover the entire tumor volume identified on T2-weighted images. A series of 60 multisection acquisitions was acquired at 1-second intervals. The first 10 acquisitions were performed before contrast agent (Magnevist; Berlex Laboratories, Wayne,

NJ) was injected to establish a precontrast baseline. At the 10th acquisition, gadopentetate dimeglumine (0.1 mmol/kg) was injected with a power injector (Medrad, Pittsburgh, PA) at a rate of 5 mL/s through an 18- or 20-gauge intravenous catheter. The injection was immediately followed by a bolus injection of sodium chloride solution (total of 20 mL at 5 mL/s).

3D T1-Weighted Imaging with Volumetric Interpolated Brain Examination.—The 3D datasets were acquired immediately after perfusion imaging. The 3D sequence used, originally designed for rapid abdominal imaging (9), was modified to obtain the high resolution necessary for brain imaging and was referred to here as volumetric interpolated brain examination (VIBE) (10). The VIBE sequence is a radio-frequency spoiled 3D GRE sequence (8..8/4.4; flip angle, 18°). The data were acquired in the sagittal projection with an FOV of 210 × 210 mm. The slab thickness was 160 mm, and the data matrix was 256 (read) × 192 (phase) × 90 (partition). Sampling was symmetric in the read- and phase-encoding directions, giving voxel dimensions of 0.82 × 1.09 mm. In the partition direction, the center of k-space occurred at line 21/90. Before Fourier transformation, the partition direction was zero-filled to 180 points. Zero filling is equivalent to interpolation and combined with asymmetric sampling gives improved spatial resolution (11). Although calculation of the exact voxel width is difficult, the width lies between 0.89 mm (FOV of 160/180 partitions after zero filling) and 1.78 mm (FOV of 160/90 partitions). Other parameters were as follows: bandwidth of 260 Hz per pixel; number of signal averages, 1; and an acquisition time of 2 minutes 20 seconds.

Conventional MR Imaging.—In all patients, conventional axial T2-weighted images (3400/119) and pre- and postcontrast axial T1-weighted MR images (600/14) of the brain were obtained.

MR Image Postprocessing

Perfusion MR Images.—The echo-planar images were transferred to an Ultra 10 workstation (Sun Microsystems, Mountain View, CA) for postprocessing. Cerebral blood volume (CBV) values were calculated from the pMRI data by using software developed in-house in the C and IDL (Research Systems, Inc, Boulder, CO) programming languages. Knopp et al (6) fully described the details of data processing, and only a summary is given in this article. During the first pass of the bolus of paramagnetic contrast agent, the signal intensity on the T2*-weighted images decreases. The gadolinium concentration can be calculated from the signal-intensity changes to obtain a plot of tissue gadolinium concentration over time. The area under this curve is proportional to the regional CBV (12). Correction for contrast material recirculation and leakage (which invalidates the CBV calculation) was performed by subtracting a baseline value from under the contrast-bolus curve. The CBV was expressed relative to an internal reference (relative CBV [rCBV]), of normal-appearing contralateral white matter.

In practice, the observer (S.G.W.) evaluated the perfusion raw-data and formed color maps in a standardized fashion. CBV values lying between a threshold rCBV of 1.25 and a maximum rCBV of 5 (in relation to normal-appearing contralateral white matter) were displayed on a green-to-red color scale. The observer then picked 10 regions of interest (diameter, 3.6 mm) where high rCBV values could potentially be found. The highest rCBV value was recorded.

VIBE images.—Observers (M.L., P.K.N.) examined the VIBE images on a satellite workstation of the MR unit by using commercially available software (Argus 04; Siemens Medical Systems). Source images and multiplanar reconstructions were analyzed in conjunction with subvolume MIP slabs. The software allowed reconstruction of subvolume MIPs positioned from source and multiplanar images. Subvolume obliquity, position, and thickness could be changed interactively and in real time. The readers were free to manipulate the MIP images to

achieve the optimal view of the vessels of interest. The typical time for the interpretation of one data set at the satellite workstation was 5–7 minutes.

Digital Subtraction Angiography

DSA was performed by means of femoral artery catheterization in all 22 patients. In all patients, a profile and half-axial projection series of the carotid artery on the ipsilateral side of the tumor was available (internal carotid artery in 15 patients, common carotid artery in seven patients). Projection series of the posterior circulation were available in six patients, and a selective angiogram of the external carotid circulation was available in one patient. Carotid artery angiograms included stereoscopic views of both the arterial phase and the venous phase.

Data Analysis

An interventional neuroradiologist (P.K.N.) who was blinded to the histopathologic diagnosis evaluated tumor vascularity on the conventional angiograms according to the following scale: 0 indicated occult; 1, mild blush; 2, moderate; and 3, exuberant. The presence of early venous return was also noted. A diagnostic neuroradiologist (S.G.W.), blinded to all imaging modalities except the conventional T1- and T2-weighted images, evaluated the MR perfusion studies to determine the maximum rCBV value for each tumor. This observer also estimated the tumor volume by multiplying the product of the three largest perpendicular lesion diameters by 0.5 and rated the contrast enhancement of the tumors as absent (no), minimal, or intense (yes). This analysis was performed on T1-weighted spin-echo images, and tumor values were recorded separately for the contrast-enhancing part of the tumor and for the region of T2 signal intensity abnormality in nonenhancing low-grade tumors.

To determine the utility of VIBE, the vessels of importance in surgical planning were individually chosen for each patient. An experienced neurosurgeon (J.G.) examined conventional T1- and T2-weighted images to select the critical vessels on the basis of the location of the tumor and the neurosurgical approach. The neurosurgeon was blinded to the VIBE and DSA images. Later, two experienced readers (P.K.N., M.L.), an interventional neuroradiologist (P.K.N.) and a diagnostic neuroradiologist (S.G.W.) blinded to the conventional angiograms, and the neurosurgeon evaluated the depiction of the vessels on the VIBE images. Visualization of *each* critical vessel on the VIBE images was then determined by consensus by using the three following categories: All indicated that VIBE imaging provided all relevant information; none, VIBE imaging provided no relevant information; and partial, VIBE imaging provided not all but some relevant information.

Immediately after this assessment, the same three observers assessed the conventional angiograms with the VIBE images to determine the agreement between DSA and VIBE, the initial rating notwithstanding. They decided whether the "partial" and "all" categories were correctly applied and whether the required information was seen in retrospect when the VIBE had been rated as providing no relevant information.

T1- and T2-weighted images were not included in the evaluation of vascular visualization. The spatial resolution of these acquisitions was not as high as that of the VIBE acquisition; therefore, these images were thought to be unlikely to provide much additional information about the vessels.

Finally, the results for the display of the arteries and veins were summarized for each patient. An overall category was scored in patients in whom multiple veins and arteries were evaluated. This overall category was scored separately for veins and for arteries as follows: All was scored when VIBE provided all of the relevant information about all vessels; none, when VIBE provided none of the relevant information on any vessel; and partial was used in other cases.

After evaluating the visualization of vascular structures, the same three observers determined whether the tumor was visible on the VIBE images and whether contrast enhancement depicted on conventional T1-weighted images was also depicted on the VIBE images.

The neurosurgeon had operated on two of the patients, and the interventional neuroradiologist had supervised the fellows performing the DSA in all cases. Image evaluation for this study occurred at least 4 weeks after the initial clinical assessment of the images.

The Spearman rank correlation coefficient test (SPSS 9.0; SPSS, Chicago, IL) was used to compare the relation between the rCBV values, the vascularity score for DSA, and the tumor size. A P value of less than .05 was considered to indicate a statistically significant difference.

Results

The study group consisted of 12 female patients and 10 male patients. The patients' ages ranged from 30 to 68 years, with a mean age of 46.9 years. Table 1 lists the histopathologic diagnoses, and Table 2 lists the locations of all tumors. Patients 9 and 18 had recurrent tumor, and all other patients had no prior brain surgery. The tumor volumes were 4–99 cm^3 (mean, 29 cm^3). The volumes of the tumors that showed contrast enhancement ranged from 1 to 32 cm^3 (mean, 9 cm^3); three tumors were not enhancing.

Comparison of Tumor Vascularity with pMRI versus DSA

A statistically significant correlation was observed between the scores for tumor blush on conventional angiograms and the MR imaging rCBV measurements ($r = 0.75$; $P < .01$) (Table 1; Figs 1 and 2). Five tumors were not directly visible at conventional angiography; these included a recurrent anaplastic astrocytoma with a markedly increased rCBV of 5.2 in a small area of the tumor. Tumors visible at conventional angiography had an rCBV of a least 1.8. The averaged rCBV for the four tumors with early venous return (arteriovenous shunting) that were visible on conventional angiograms was 18.6 ± 7.6. No significant correlation was observed between the total tumor volumes and the rCBV values ($r = 0.10$, $P > .05$) or between the total tumor volumes and the DSA vascularity score ($r = -0.23$, $P > .05$). The volume of the contrast-enhancing region did not correlate with the rCBV ($r = 0.41$, $P > .05$), but it did correlate with the DSA vascularity score ($r = 0.66$, $P < .01$). The two tumors that had been scored as not visible (score 0) or as only mildly hyperperfused (score 1) at DSA, but they showed the highest rCBV values in their respective DSA scoring group. Both had small contrast-enhancing tumor volumes of 1 and 2 cm^3.

Comparison of Critical Brain Vessels with VIBE versus DSA

A total of 76 venous structures and arteries were evaluated. Table 2 lists the location of the tumors and the neurosurgical approach for each patient, with the vascular structures that were of interest for neurosur-

TABLE 1: Histopathology, contrast enhancement, and comparison of rCBV and vascularity score on DSA images of 22 tumors

Patient No.	Histopathology	Contrast Enhancement	rCBV	Vascularity on DSA Image
1	Mixed glioma (low grade)	No	1.0	0
2	Mixed glioma (low grade)	No	1.1	0
3	Leiomyosarcoma (metastasis)	Yes	1.8	1
4	Glioblastoma multiforme	Yes	2.4	1
5	Anaplastic astrocytoma	Yes	2.6	0
6	Mixed glioma (low grade)	No	2.7	0
7	Meningioma	Yes	4.1	2
8	Oligodendroglioma (anaplastic)	Yes	4.7	1
9	Mixed glioma (anaplastic)	Minimal	5.2	0
10	Anaplastic astrocytoma	Yes	6.1	2
11	Glioblastoma multiforme	Yes	6.2	2
12	Mixed glioma (anaplastic)	Yes	7.6	2*
13	Glioblastoma multiforme	Minimal	8.6	1
14	Adenocarcinoma (metastasis)	Yes	10.3	2
15	Meningioma	Yes	11.8	2
16	Glioblastoma multiforme	Yes	12.6	2
17	Mixed neuroepithelial tumor (anaplastic)	Minimal	13.4	1
18	Glioblastoma multiforme	Yes	14.2	2
19	Glioblastoma multiforme	Yes	19.5	3*
20	Glioblastoma multiforme	Yes	23.6	3*
21	Glioblastoma multiforme	Yes	23.8	2
22	Glioblastoma multiforme	Yes	23.9	2*

* Arteriovenous shunting was present.

TABLE 2: Tumor location, surgical approach, and critical vessels evaluated in 22 tumors

Patient No.	Location and Side	Surgical Approach	Vessels Evaluated*	Arterial Segments Evaluated
1	Temporal, L	Pterional	Cortical veins	MCA (2–4)
2	Temporal, R	Temporal craniotomy	Cortical veins	None
3	Tectal	Stereotactic biopsy	Cortical veins, ISS, deep venous system	PCA, SCA
4	Temporal, L	Stereotactic biopsy	Cortical veins	MCA (2–4), AchA, Pch
5	Parietal, L	Stereotactic biopsy	Cortical veins, deep venous system	None
6	High parietal, L	Parietal craniotomy		None
7	Cerebellopontine, L	Transpetrosal	Cortical veins, sigmoid sinus, SPS	PCA, Pcom, SCA, AICA, PICA
8	Frontal, L	Frontal craniotomy	Cortical veins, ISS, IV, deep venous system	ACA (2–4)
9	Parietal, R	Posterior frontal craniotomy	Cortical veins	MCA (2–4)
10	Frontal, R	Frontal craniotomy	Cortical veins, SSS	None
11	Frontal, R	Frontal craniotomy	Cortical veins, IV	ACA (2–4), MCA (2–4)
12	Insula, L	Posterior frontal craniotomy	Cortical veins	MCA (4)
13	Frontal, R	Frontal craniotomy	Cortical veins	ACA (2–4)
14	High parietal, L	Frontal craniotomy	Cortical veins	MCA (4)
15	Parasagittal, L	Frontal craniotomy	Cortical veins, SSS, IV	None
16	Parietal, L	Parietal craniotomy	Cortical veins, IV	None
17	High parietal, L	Stereotactic biopsy	Cortical veins, ISS, IV	ACA (2–4)
18	High occipital, L	Superior parietal lobule	Cortical veins, SSV, IV	ACA (2–4)
19	Parietotemporal, L	Posterior temporal craniotomy	Cortical veins	None
20	Thalamic, L	Transcortical	Cortical veins, deep venous system	AchA, PchA, thalamoperforators
21	Frontal, L	Frontal craniotomy	Cortical veins, IV	ACA (3–4)
22	Occipital, L	Occipital craniotomy	Cortical veins, SSS, IV	None

* ISS indicates inferior sagittal sinus; SPS, superior petrosal sinus; IV, interhemispheric veins; and SSS, superior sagittal sinus.

† ACA indicates anterior cerebral artery; Acha, anterior choroidal artery; AICA, anterior inferior cerebellar artery; MCA, middle cerebral artery; PCA, posterior cerebral artery; Pcha, posterior choroidal artery; Pcom, posterior communicating artery; PICA, posterior inferior cerebellar artery; and SCA, superior cerebellar artery.

gical planning. In all patients, the venous structures were evaluated. In 14 patients, the arteries were also assessed. Table 3 shows the summarized score of the blinded readout and the scoring scheme for the different venous structures.

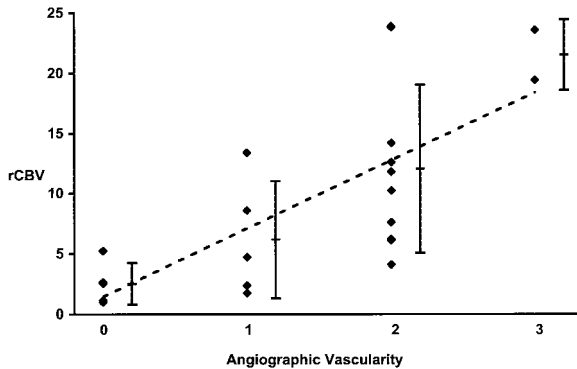*Venous System.*—In 17 patients (77%), VIBE pro-

FIG 1. Relationship between maximum rCBV and angiographic vascularity. Scores are as follows: 0 indicates occult; 1, mild blush; 2, moderate blush; and 3, exuberant. The correlation between the two parameters is shown by the *dotted line* ($r = 0.75$; $P < .05$). The average rCBV and the standard deviation are displayed for each group of angiographic vascularity scores.

vided all the relevant information about the venous system. In the remaining five patients (23%), VIBE provided partial information. Cortical veins were assessed in all patients; the veins were well visualized in 18 of the 22 patients, and partial information was obtained in four (Fig 2 and 3). Information about the interhemispheric veins was rated as complete in seven cases and as partial in one case. In all of the cases scored as providing partial information, assessment of the patency and course of the vessels was difficult because of the blending of the veins with the adjacent contrast-enhancing parts of the tumor (Fig 4). VIBE provided all of the relevant information about the large venous sinuses (Figs 3 and 5) and the deep venous structures. In the four patients in whom the deep venous structures were deemed relevant, the vessels compromised the internal cerebral veins (all patients), the basal vein of Rosenthal (patients 3, 5, 20), the thalamostriate veins (patients 3, 8, 20), the vein of Galen and the precentral vein (patient 3), and the septal veins (patient 8).

When the VIBE images were reviewed with the DSA images as the standard of reference, all evaluated vascular structures were found to have been scored correctly. That is, in all patients, when VIBE images were scored as providing all or partial information about the venous system, DSA did not provide different information.

Arteries.—In all patients, VIBE images did not provide all of the information retrievable with conventional angiography. In seven patients (50%), the information was scored as being partial, and in the other seven patients, the information retrievable on the VIBE images was scored as being irrelevant or absent. As for the veins, all evaluated vascular structures had been scored in the correct category, and no misleading information had been retrieved. Information was available in cases in which the main arterial structures of the circle of Willis or of its proximal branches in relation to the tumor were important (Fig 5). However, small arteries such as the thalamoper-

forating and choroidal arteries were not visualized. The course of the more distal cerebral arteries (from the second segment to the fourth segment of the cerebral arteries) was not seen on VIBE images, or they could not be distinguished from small adjacent veins. Importantly, the identification of the terminal branches (eg, Rolandic artery) in relation to the tumor was not possible.

All tumors were visualized on the VIBE images, and a pattern of contrast enhancement similar to that seen on the T1-weighted images was found. Evaluation of a VIBE 3D data set required about 15 minutes at the beginning of the study, but with more experience, this time decreased to 5 minutes.

Discussion

In this study, the assessment of tumor vasculature by using an MR protocol with commercially available sequences and a measurement time of less than 4 minutes was compared with the assessment with conventional DSA.

Tumor (neo-) vascularity was assessed by measuring CBV with dynamic contrast-enhanced pMRI. Previous investigations have shown that this technique has great potential in the evaluation of intracranial mass lesions. Results of comparisons of MR imaging findings and histopathologic features suggest that the quantitative estimates of CBV reflect the underlying microvasculature (5, 6). Furthermore, Sugahara et al (8) have shown that perfusion-sensitive MR imaging findings are correlated with DSA findings in patients with gliomas. Here, we compared pMRI and DSA in a study population with a variety of tumors and found a similar correlation between the rCBV values and the tumor blush on DSA images. We also evaluated the possible influence of tumor size on the ability to detect tumor (neo-) vascularity. Although DSA offers spatial resolution much better than that of pMRI, we found markedly elevated rCBV values in two tumors that were invisible or that showed only mild tumor blush on DSA images. In both of these cases, which involved high-grade tumors, the contrast-enhancing regions containing the area of abnormal perfusion were small. We assume that these small tumor parts were not seen on the DSA images because of the superimposition of normal vascular structures. Unlike DSA, a projection technique, cross-sectional visualization with pMRI may be better for the detection of small foci of increased vascularity. This hypothesis is supported by the significant correlation between DSA vascularity score and the volume of contrast-enhancing tumor. No such correlation was found between rCBV values and contrast-enhancing tumor volume. One limitation of this argument is that the contrast-enhancing tumor region does not necessarily indicate the area of the highest tumor vascularity, but rather, it may indicate the volume of the tumor with a disrupted blood-brain barrier. On the other hand, the highest rCBV values are generally found in areas of contrast enhancement.
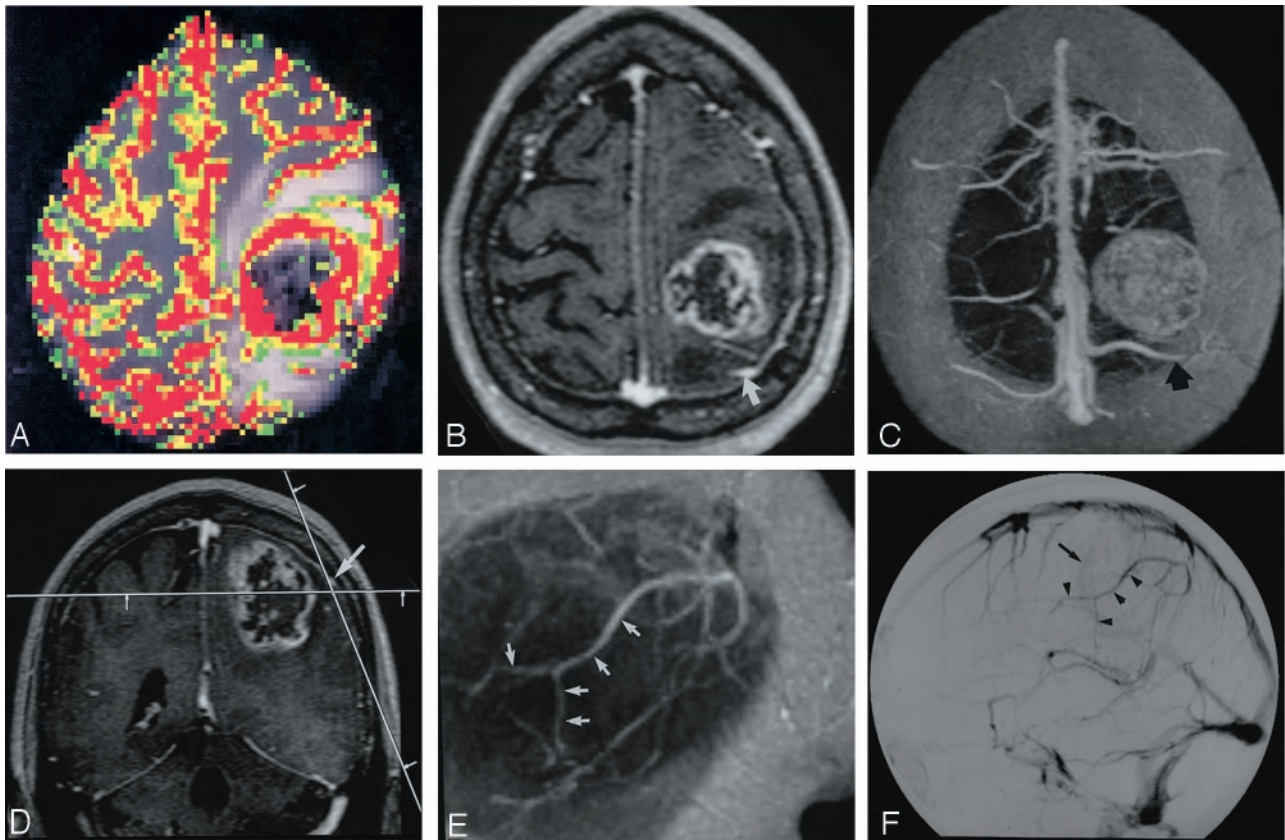
The VIBE sequence used to evaluate large vessels

FIG 2.   Images in a 57-year-old patient with left parietal glioblastoma multiforme.

A, Color overlay map reconstructed from pMRI (1000/54) shows marked hyperperfusion of the lesion compared with normal white matter.

B, Para-axial source image of the 3D VIBE acquisition (8.8/4.4; flip angle, 18°) shows a contrast-enhancing tumor with a necrotic center. Note the prominent cerebral vein posterior to the tumor (*arrow*).

C, Real-time MIP image with 30-mm thickness was reconstructed in position of the image in *A* and shows the relation of the tumor to the cortical veins and the superior sagittal sinus. The more distal part of the overlying cortical vein (*arrow*) is not included in the volume. As a result of the MIP algorithm, the tumor appears solid.

D, Coronal source image shows an overlying cortical vein (*arrow*) in relation to the tumor. The line in parasagittal plane shows the orientation of the image in *E.*

E, Real-time parasagittal MIP image with 10-mm thickness shows the distal part of the vein in its course (*arrows*).

F, Venous-phase DSA image obtained with an injection in the left internal carotid artery shows persistent tumor blush (*arrow*). Compare the display of the overlying cortical vein (*arrowheads*) to the image in *E.*

TABLE 3: Scoring table for vascular information provided on VIBE images with DSA as the standard of reference

Vascular Structure	No. of Patients	Score*		
		All	Partial	None
Total veins	22	17	5	0
Cortical veins	22	18	4	0
Interhemispheric veins	8	7	1	0
Venous sinuses	8	8	0	0
Deep venous system	4	4	0	0
Total arteries	14	0	7	7

* Scores were as follows: All indicated that VIBE imaging provided all of the relevant information; partial, VIBE imaging provided some but not all of the relevant information; and none, VIBE imaging provided none of the relevant information.

involved zero filling, a method of interpolation that was previously used in fast 3D MR angiography to reduce partial-volume artifacts in MIP images (13). In this instance, however, zero filling is used in combination with asymmetric sampling to improve spatial resolution. It was thus possible to cover the entire head with an almost isotropic resolution of 1 mm³ in

little more than 2 minutes. As the VIBE data set was acquired after the perfusion sequence, arteries and veins as well as the contrast-enhancing parts of the tumor were enhanced. However, we were able to interactively follow the vascular structures by scrolling through two-dimensional (2D) reconstructions derived in real time from the volumetric data sets. This
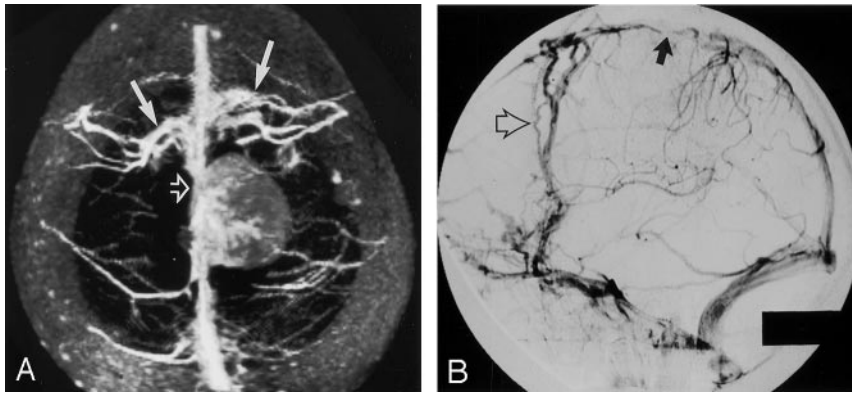
FIG 3. Images in a 46-year-old patient with left parasagittal meningioma.

A, Real-time para-axial MIP image with 30-mm thickness shows occlusion (*open arrow*) of the superior sagittal sinus by the tumor, which has lower signal intensity compared with that of the sinus. Note the extensive collateral cortical veins (*solid arrows*) draining the frontal part of the sinus.

B, Venous-phase DSA obtained with an injection in the left common carotid artery shows occlusion of the sinus (*solid arrow*) and prominent frontal collateral cortical veins (*open arrow*).

ability greatly aids the reader in distinguishing arteries and veins. Because the voxel volume was nearly isotropic, these 2D reconstructions have almost the same quality as the sagittal source images. Similarly, the ability to interactively define 3D volumes with any desired orientation and with any desired slab thickness for targeted MIP images proved to be of considerable value in rapidly gaining an overview of areas of interest without time-consuming manual editing of the data. The ability to switch from the source data to 2D reconstructions to targeted 3D MIP reconstructions in real time was also invaluable.

Even by using postprocessing techniques such as these, assessment of the course of the vessels was not possible when smaller vascular structures blended

FIG 4. Sagittal (*A*) and parasagittal (*B*) images in a 44-year-old patient with recurrent left parietal glioblastoma multiforme. Sagittal source images lateral to the contrast-enhancing part of the tumor show a cortical vein (*large arrow*), which blends with the tumor in the medial part (*small arrows* in *B*) and can not be distinguished from the tumor. On conventional angiograms (not shown), the vein was patent.

with contrast-enhancing parts of the tumor. Furthermore, we could not follow the course of small distal arterial branches because of the superimposition of small veins and the limited spatial resolution.

On the other hand, we could identify the large proximal arteries and obtain a good overall delineation of the venous structures on VIBE images. This result can be attributed mainly to the larger size of most of the venous structures evaluated. We could also distinguish the two meningiomas from the venous sinuses because of their lower enhancement in comparison to that of the vein. Therefore, the diagnosis of an occlusion in one of the cases was based not only on the signal-intensity characteristics but also on the extensive collateral circulation visualized, which indicated, at least, a severe functional impairment of the regular drainage pattern. However, the ability of VIBE to aid in the assessment of venous occlusion or invasion by tumors must be verified with further studies.

Our comparison of VIBE and DSA had some limitations. First, vessels regarded as important for surgical planning were selected by a single neurosurgeon who was accustomed to using DSA for evaluating vascular anatomy. This method may have introduced a bias in favor of DSA. Neurosurgeons who are relatively unfamiliar with DSA might have chosen other vessels, depending on their favored surgical approach.

Second, the VIBE images were interpreted by consensus so that no assessment of interobserver reliability was possible. On the other hand, consensus review minimizes interpretation errors that may result from relative inexperience in interpreting vascular 3D MR data. Specialists with expertise in interpreting vascular 3D MR studies may not have a complete knowledge of the intricacies and implications of certain findings in evaluating cerebral vascular structures for neurosurgical planning. Likewise, neurosurgeons and specialists with expertise in interpreting DSA studies may not be skilled in interpreting MR studies.

Third, we evaluated only the vessels that were regarded as being important for the neurosurgical approach. In a previous study of MR angiography in patients with brain tumors (14), the evaluation criteria were more standardized, but the investigators focused mainly on the visualization of larger arteries and veins. Therefore, this more standardized approach
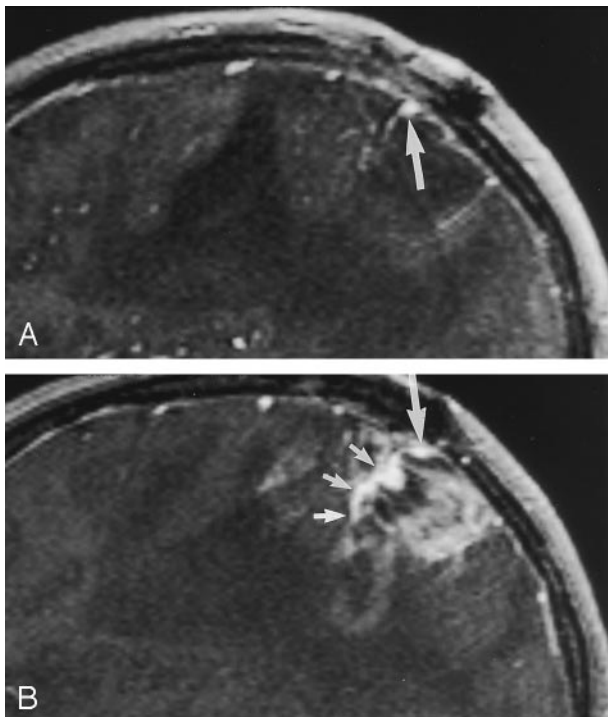
FIG 5. Images in a 42-year-old patient with meningioma in right cerebellopontine angle.

A, Real-time para-axial MIP image with 15-mm thickness shows the sigmoid sinus (small arrows) in relation to a meningioma (large arrow), which has signal intensity lower than that of the sinus. No signs of tumor infiltration are depicted.

B, Real-time paracoronal MIP image with 2-mm thickness shows the relation of the posterior fossa arteries to the tumor. Gaps in the basilar artery (large horizontal arrows) and in the right posterior cerebral artery (large vertical arrow) are due to partial volume effects. The proximal superior cerebellar artery is shown with great detail (small arrows).
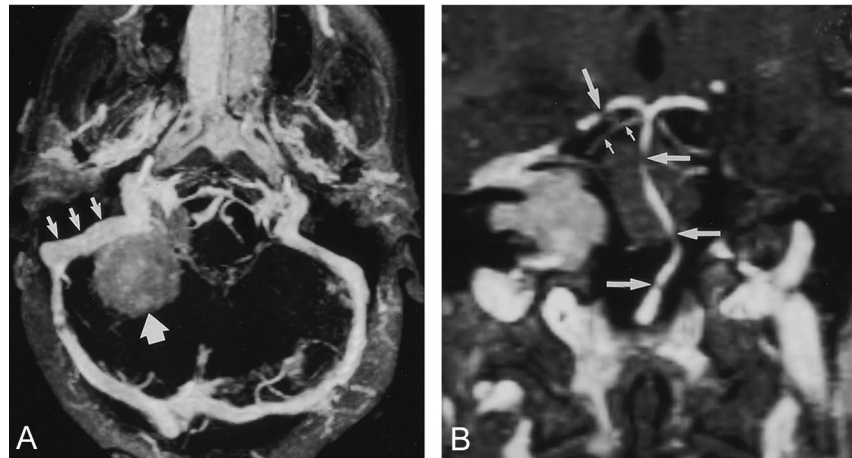
might not have allowed adequate assessment of the technique in small but clinically relevant vessels.

Finally, the VIBE sequence that we used had limited spatial resolution. Small-vessel delineation, especially depiction of the arteries, would have been improved by using a sequence with higher spatial resolution. However, this change would not overcome the principal problem of blending between contrast-enhancing regions of the tumor and adjacent vessels or between small adjacent arteries and veins. Moreover, increased spatial resolution would reduce the signal-to-noise ratio, and longer imaging times would be required. In the future, improvements in VIBE acquisition times by using fast-imaging techniques such as sensitivity encoding (SENSE) or simultaneous acquisition of spatial harmonics (SMASH) (15, 16) may improve the spatial resolution with the same imaging time. Alternative magnetic resonance angiographic (MRA) methods such as high-resolution time-of-flight imaging with venous saturation pulses might improve visualization of the arteries when blending occurs between arteries and veins or contrast-enhancing structures. However, such sequences require relatively long examination times, and additional MRA sequences would still be required to visualize veins. We therefore focused on only the fast VIBE sequence.

Finally, the possible *advantages* of VIBE over DSA, including the ability to obtain different views of vessels and cross-sectional images of brain vessels and tumor, were not addressed in this study. Determining whether presurgical angiography of any type results in improved patient outcome or whether the additional information provided by DSA justifies the cost and risk of that procedure is beyond the scope of this investigation. Such studies are clearly of interest.

Conclusion

A fast imaging protocol, including VIBE and pMRI, provides some of the information about tumor (neo-) vascularity and adjacent vascular anatomy that can be obtained by conventional angiography. However, major limitations of MR compared with DSA is the blending of vascular structures with contrast-enhancing tumor parts and an insufficient depiction of distal cerebral arteries.

References

1. Masters LT, Pryor JC, Nelson PK. **Angiographic findings associated with intra-axial intracranial tumors.** *Neuroimaging Clin N Am* 1996;6:739–749
2. Cloft HJ, Joseph GJ, Dion JE. **Risk of cerebral angiography in patients with subarachnoid hemorrhage, cerebral aneurysm, and arteriovenous malformation: a meta-analysis.** *Stroke* 1999;30:317–320
3. Lev MH, Rosen BR. **Clinical applications of intracranial perfusion MR imaging.** *Neuroimaging Clin N Am* 1999;9:309–331
4. Wong JC, Provenzale JM, Petrella JR. **Perfusion MR imaging of brain neoplasms.** *AJR Am J Roentgenol* 2000;174:1147–1157
5. Aronen HJ, Gazit IE, Louis DN, et al. **Cerebral blood volume maps of gliomas: comparison with tumor grade and histologic findings.** *Radiology* 1994;191:41–51
6. Knopp EA, Cha S, Johnson G, et al. **Glial neoplasms: dynamic contrast-enhanced T2*-weighted MR imaging.** *Radiology* 1999;211:791–798
7. Sugahara T, Korogi Y, Shigematsu Y, et al. **Perfusion-sensitive MRI of cerebral lymphomas: a preliminary report.** *J Comput Assist Tomogr* 1999;23:232–237
8. Sugahara T, Korogi Y, Kochi M, et al. **Correlation of MR imaging-determined cerebral blood volume maps with histologic and angiographic determination of vascularity of gliomas.** *AJR Am J Roentgenol* 1998;171:1479–1486
9. Rofsky NM, Lee VS, Laub G, et al. **Abdominal MR imaging with a volumetric interpolated breath-hold examination.** *Radiology* 1999;212:876–884
10. Wetzel SG, Johnson G Tan AGS, et al. **Three-dimensional, T1-weighted gradient-echo imaging of the brain with a volumetric interpolated examination.** *AJNR Am J Neuroradiol* 2002;23:995–1002
11. Hurst GC, Hua J, Simonetti OP, et al. **Signal-to-noise, resolution, and bias function analysis of asymmetric sampling with zero-padded magnitude FT reconstruction.** *Magn Reson Med* 1992;27:247–269
12. Rosen BR, Belliveau JW, Vevea JM, et al. **Perfusion imaging with NMR contrast agents.** *Magn Reson Med* 1990;14:249–265
13. Du YP, Parker DL, Davis WL, et al. **Reduction of partial-volume artifacts with zero-filled interpolation in three-dimensional MR angiography.** *J Magn Reson Imaging* 1994;4:733–741
14. Wilms G, Bosmans H, Marchal G, et al. **Magnetic resonance angiography of supratentorial tumors: comparison with selective digital subtraction angiography.** *Neuroradiology* 1995;37:42–47
15. Weiger M, Pruessmann KP, Kassner A, et al. **Contrast-enhanced 3D MRA using SENSE.** *J Magn Reson Imaging* 2000;12:671–677
16. Sodickson DK, Manning WJ. **Simultaneous acquisition of spatial harmonics (SMASH): fast imaging with radiofrequency coil arrays.** *Magn Reson Med* 1997;38:591–603